doi: 10.82124/CEAS-GNC-2026-089 CEAS-GNC-2026-089

Incremental Differential Proportional–Integral (iDPI) Control for Lateral Motion: A Model-Following Approach

Marwan Shalaby Graduate Researcher, Institute of Flight System Dynamics, Technical University of Munich, Munich, Germany. m.shalaby@tum.de
Flight Dynamics and Control Engineer, Textron Aviation, Munich, Germany. mshalaby@txt.textron.com

Agnes Steinert Postdoctoral Researcher, Institute of Flight System Dynamics, Technical University of Munich, Munich, Germany. agnes.steinert@tum.de

David Basta Graduate Researcher, Institute of Flight System Dynamics, Technical University of Munich, Munich, Germany. david.s.shawky@gmail.com

Florian Holzapfel Professor and Head of the Institute of Flight System Dynamics, Technical University of Munich, Munich, Germany. florian.holzapfel@tum.de

ABSTRACT

Incremental Nonlinear Dynamic Inversion (INDI) has gained popularity in various aerospace control applications, as it reduces reliance on accurate models and improves disturbance rejection. Recently, the incremental control approach has been combined with classical proportional-integral (PI) control to increase robustness, avoid hidden coupling terms, and enable fast gain scheduling, in a manner similar to the differential PI (DPI) controller. This paper extends the incremental DPI (iDPI) concept to a model-following structure for MIMO systems in the context of fixed-wing flight control. It compares a coupled and a simplified decoupled physical reference model as well as different error controller structures. The approach is evaluated using a high-fidelity six-degree-of-freedom (6-DoF) simulation model of a commercial aircraft, including several practical adaptations to support real-world implementation. The results highlight the suitability of the proposed iDPI framework in achieving robust, implementable flight controllers.

Keywords: Incremental Nonlinear Dynamic Inversion (INDI), Incremental Differential PI (iDPI), Incremental control, Model-following control, Flight control, MIMO systems, Robust control, Gain scheduling, Fixed-wing aircraft, Nonlinear control

1 Introduction

Incremental Nonlinear Dynamic Inversion (INDI) was introduced to overcome key limitations of classical Nonlinear Dynamic Inversion (NDI). While NDI relies heavily on accurate model knowledge, INDI utilizes sensor-based feedback, which reduces its dependency on accurate models, resulting in improved disturbance rejection and enabling control of input non-affine systems such as VTOL aircraft

*The first two authors contributed equally to this paper.

with tilting rotors. In addition, it adopts a model-following structure in which the desired closed-loop behavior is defined by a tunable reference model, independently of disturbance rejection and robustness. This separation facilitates controller synthesis and analysis and simplifies the process of meeting performance and handling quality requirements. These advantages have made INDI particularly attractive for novel aircraft configurations, where exact model information is often incomplete or costly to obtain. Over the past decade, research on INDI has expanded rapidly across both aerospace and non-aerospace domains, leading to numerous applications and several advanced variants [1–4]. Two recent survey papers provide a comprehensive overview of the evolution of INDI, its variants, and its applications across different vehicle types and control loops [5, 6].

Differential PI (DPI) features the ability to avoid the hidden coupling effects that gain scheduling can introduce [7]. It supports scheduling of controller gains over rapidly varying states, such as the angle of attack, and has been successfully applied in the Eurofighter [8]. Building on the concepts of INDI and DPI, the Incremental DPI (iDPI) framework was proposed and subsequently validated in flight tests [9, 10] where it was shown that iDPI outperforms DPI in the longitudinal control of a fixed-wing model aircraft. More recently, this comparison was extended to MIMO systems in [11], where a lateral motion controller for an aircraft was evaluated under two actuator loop configurations, one relying on direct actuator measurements and the other employing an actuator model.

The iDPI framework can be further enhanced by embedding it within a model-following structure. This motivates the investigation of how such a model-following structure can be systematically formulated for MIMO flight control systems while retaining the practical advantages of the incremental approach. In this paper, we:

- Extend the iDPI architecture to a model-following structure for MIMO systems using a physical reference model.
- Investigate two types of reference models, decoupled and physically coupled, and analyze their impact on tracking and robustness under model uncertainty.
- Analyze different error controller structures.
- Adapt the model-following iDPI for practical implementation and demonstrate its applicability on a high-fidelity 6-DoF nonlinear simulation model of a commercial aircraft.

2 Aircraft Lateral Motion Model

We analyze the lateral motion of a fixed-wing aircraft in steady, level flight, represented here by a linear time-invariant (LTI) model:

$$\begin{bmatrix} \dot{r} \\ \dot{\beta} \\ \dot{p} \\ \dot{\phi} \end{bmatrix} = \begin{bmatrix} N_r & N_\beta & N_p & 0 \\ Y_r - 1 & Y_\beta & Y_p & \frac{g}{V_0} \\ L_r & L_\beta & L_p & 0 \\ 0 & 0 & 1 & 0 \end{bmatrix} \begin{bmatrix} r \\ \beta \\ p \\ \phi \end{bmatrix} + \begin{bmatrix} N_\xi & N_\zeta \\ Y_\xi & Y_\zeta \\ L_\xi & L_\zeta \\ 0 & 0 \end{bmatrix} \begin{bmatrix} \xi \\ \zeta \end{bmatrix} + \begin{bmatrix} -\frac{N_\beta}{V_0} & -N_p & -N_r \\ -\frac{Y_\beta}{V_0} & -Y_p & -Y_r \\ -\frac{L_\beta}{V_0} & -L_p & -L_r \\ 0 & 0 & 0 \end{bmatrix} \begin{bmatrix} v_g \\ p_g \\ r_g \end{bmatrix} \tag{1}$$

In this formulation, r denotes the yaw rate, β the sideslip angle, p the roll rate, and ϕ the bank angle. The control inputs are the aileron deflection ξ and rudder deflection ζ. External disturbances are introduced through the lateral gust velocity v_g, gust-induced roll rate p_g, and gust-induced yaw rate r_g. The objective of the control design is to ensure precise tracking of commanded ϕ and β, with dynamics shaped according to handling qualities criteria, in the presence of disturbances and model uncertainties.

3 Model-Following Control

3.1 Motivation

The key advantage of model-following control is that it decouples the definition of the desired system behavior from the handling of disturbances and model uncertainties. The desired response is fully defined by the reference model, which can be tuned according to handling quality requirements or performance goals. As a result, the feedforward signal drives the system toward this ideal behavior under nominal conditions. This eliminates the need for the error controller to contribute to tracking performance under nominal conditions, reserving its role solely for disturbance rejection or to deal with model uncertainties. This separation simplifies both the tuning process for the reference model and the controller, as it allows the handling qualities, performance requirements, and disturbance rejection requirements to be treated independently.

3.2 Reference Model Variants

Utilizing a physical reference model involves designing reference signals for the inner loop controller based on the aircraft's physics, ensuring that the dynamic behavior aligns with handling quality standards. This approach facilitates the implementation of protection schemes within the reference model [12, 13]. For longitudinal motion, the physical reference model typically employs short-period dynamics. However, for lateral motion, the situation is more complex due to the coupling between the roll and yaw axes in a MIMO system. This subsection aims to investigate the following reference model variants:

- Physically Coupled: Channel interactions are preserved.
- Simplified Decoupled: Channels are treated independently.

In the model-following setup with a physical reference model, the main difference between INDI and iDPI lies in the formulation of the error controller. In such a model-following setup, the role of the error controller is to ensure stability, handle uncertainties, and reject disturbances. The following analysis focuses on tracking and the feedforward path, with the key aspect under investigation being the design of the reference model, rather than the specific error controller formulation. In the closed-loop simulations, we will employ an INDI-based error controller. A detailed investigation of the model-following iDPI structure with different error controller formulations will follow in Section 4.

3.2.1 Physically coupled reference model

Fig. 1 illustrates a "vanilla" INDI controller with a physically coupled reference plant model. This reference model is basically a copy of the linear plant dynamics. The output $\boldsymbol{y}_{ref}$ denotes the control variables roll rate p and sideslip angle β, $\boldsymbol{G}_P$ represents the plant model, and $\boldsymbol{G}_A$ is a diagonal matrix with the actuator dynamics of the aileron and rudder. A DPI-based MIMO controller is used in the reference model. This reference model controller generates $\boldsymbol{u}_{c,ref}$ to decouple the reference model internally and is tuned to ensure that the reference closed-loop dynamics meet relevant handling quality and performance criteria. DPI serves as an example of a reference model controller, for which a detailed analysis and gain synthesis procedure for fixed-wing lateral dynamics are provided in [11].

In the following, it is shown analytically that for the closed-loop dynamics under nominal conditions, the depicted choice of the feedforward signal in combination with the full coupled physical reference model ensures that the true system will track the reference model such that Eq. (2) holds.

$$\dot{\boldsymbol{y}}_{ref} = \dot{\boldsymbol{y}} \tag{2}$$

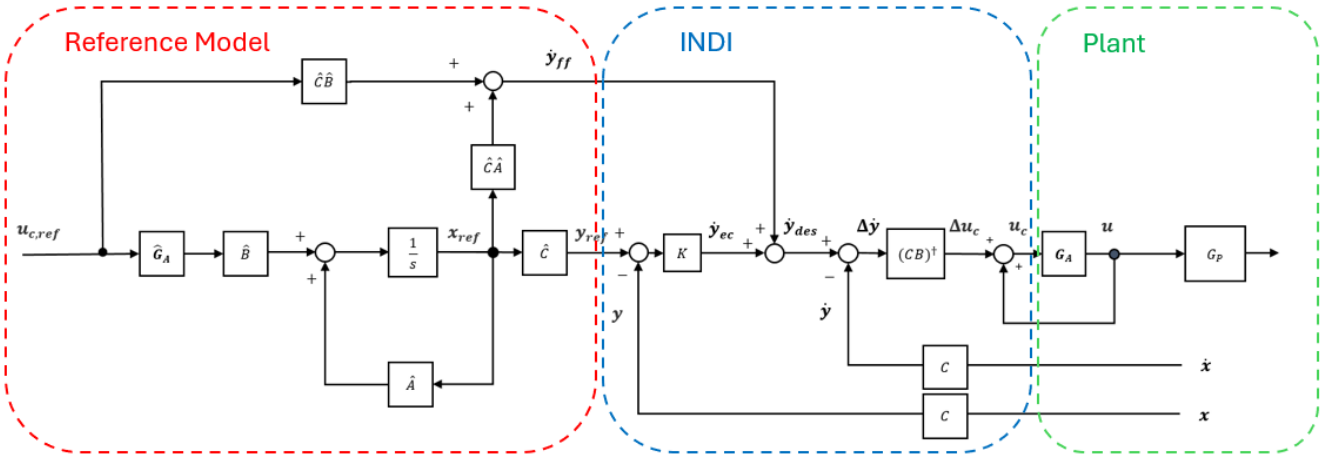

Fig. 1 Vanilla INDI with physically coupled reference model

The rate of change of the control variable can be represented as follows:

$$\begin{aligned} \dot{\boldsymbol{x}} &= A\boldsymbol{x} + B\boldsymbol{u} \\ \dot{\boldsymbol{y}} &= C\dot{\boldsymbol{x}} = CA\boldsymbol{x} + CB\boldsymbol{u} \end{aligned} \tag{3}$$

Since a full dynamic reference model is utilized:

$$\hat{A} = A, \quad \hat{B} = B, \quad \hat{C} = C = \begin{bmatrix} 1 & 0 & 0 & 0 \\ 0 & 0 & 1 & 0 \end{bmatrix} \tag{4}$$

holds under nominal conditions, where the $\hat{*}$ notation denotes the model parameters employed in the reference model. The incremental loop results in an input signal to the plant model that follows:

$$\boldsymbol{u} = \boldsymbol{G}_A(I - \boldsymbol{G}_A)^{-1}\Delta\boldsymbol{u}_c \tag{5}$$

where $\Delta\boldsymbol{u}_c$ can be represented as:

$$\Delta\boldsymbol{u}_c = (CB)^{\dagger}(\dot{\boldsymbol{y}}_{des} - \dot{\boldsymbol{y}}) \tag{6}$$

Substituting Eq. (6) and Eq. (5) into Eq. (3), while assuming that G_A is a diagonal matrix with identical entries, yields, after further simplification, the following closed-loop relation:

$$\dot{\boldsymbol{y}} = (I - G_A)CA\boldsymbol{x} + G_A\dot{\boldsymbol{y}}_{des} \tag{7}$$

The desired rate of change of the control variables is split up into a feedforward term and a simple error controller:

$$\dot{\boldsymbol{y}}_{des} = \dot{\boldsymbol{y}}_{ff} + K(\hat{C}\boldsymbol{x}_{ref} - C\boldsymbol{x}) \tag{8}$$

where the feedforward term $\dot{\boldsymbol{y}}_{ff}$ results from a fully coupled dynamic plant model of the reference model as follows:

$$\dot{\boldsymbol{y}}_{ff} = \hat{C}\hat{A}\boldsymbol{x}_{ref} + \hat{C}\hat{B}\boldsymbol{u}_{c,ref} \tag{9}$$

Substituting Eq. (9) and Eq. (8) into Eq. (7) with the assumption that the model is perfectly known, under nominal conditions ($\boldsymbol{x}_{ref} = \boldsymbol{x}$), and G_A is diagonal with equal entries, the rate of change of the control variable results in:

$$\dot{\boldsymbol{y}} = CA\boldsymbol{x} + G_A\hat{C}\hat{B}\boldsymbol{u}_{c,ref} \tag{10}$$

The reference rate of change of the control variable resulting from the full dynamic plant model of the reference model is as follows:

$$\dot{\boldsymbol{y}}_{ref} = \hat{C}\hat{A}\boldsymbol{x}_{ref} + \hat{C}\hat{B}\hat{G}_A\boldsymbol{u}_{c,ref} \tag{11}$$

Hence, Eq. (2) holds. This indicates that through careful design, a reference model utilizing a complete dynamic plant model can generate a feedforward signal that achieves perfect tracking under nominal conditions, without requiring supplementary feedback mechanisms.

3.2.2 Simplified decoupled reference model

The second investigated reference model implements the roll and yaw channels as completely decoupled and independent. The reference plant dynamics are selected as:

$$\dot{\boldsymbol{x}}_{ref} = \begin{bmatrix} N_r & N_\beta & 0 & 0 \\ -1 & Y_\beta & 0 & 0 \\ 0 & 0 & L_p & 0 \\ 0 & 0 & 1 & 0 \end{bmatrix} \cdot \boldsymbol{x}_{ref} + \boldsymbol{G}_A(s) \begin{bmatrix} \dot{r}_{c,ref} \\ 0 \\ \dot{p}_{c,ref} \\ 0 \end{bmatrix} \tag{12}$$

which corresponds to the plant dynamics in Eq. (1) with all coupling terms being removed and where the roll and yaw accelerations, produced by the control effectors, are considered as virtual inputs. These virtual input commands are produced by desired yaw and roll rate dynamics, which are decoupled. The roll rate dynamics are specified as first-order dynamics given by:

$$\dot{p}_{c,ref} = (p_c - p_{ref})\omega_p \tag{13}$$

where $\dot{p}_{ref}$ is the input to Eq. (12). In the yaw channel, linear second-order dynamics are used to generate $\ddot{\beta}_{ref}, \dot{\beta}_{ref}, \beta_{ref}$ based on a sideslip angle command β_c according to:

$$\ddot{\beta}_{ref} = -2\zeta\omega_\beta\dot{\beta}_{ref} + \omega_\beta^2(\beta_c - \beta_{ref}). \tag{14}$$

According to the reference model dynamics in Eq. (12), the second derivative of β corresponds to:

$$\ddot{\beta} = -\dot{r} + Y_\beta\dot{\beta} \tag{15}$$

Hence, we solve for $\dot{r}$ and obtain:

$$\dot{r}_{c,ref} = -\omega_\beta^2(\beta_c - \beta_{ref}) + (2\zeta\omega_\beta + Y_\beta)\dot{\beta}_{ref} \tag{16}$$

Fig. 2 reveals the corresponding block diagram of the roll and yaw dynamics. Fig. 3 shows the block diagram of the reference plant model, INDI controller, and plant. The input to the reference plant model is $\dot{\boldsymbol{x}}_{\boldsymbol{c,ref}}$, as shown in Eq. (17), with the commanded reference rates generated by the reference model controller as represented in Eq. (13) and Eq. (16).

$$\dot{\boldsymbol{x}}_{c,ref} = \left[\dot{r}_{c,ref},\ 0,\ \dot{p}_{c,ref},\ 0\right]^{\mathrm{T}} \tag{17}$$

The feedforward term for this architecture can be written as:

$$\dot{\boldsymbol{y}}_{ff} = \hat{C}\hat{A}\boldsymbol{x}_{ref} + \hat{C}\dot{\boldsymbol{x}}_{c,ref} \tag{18}$$

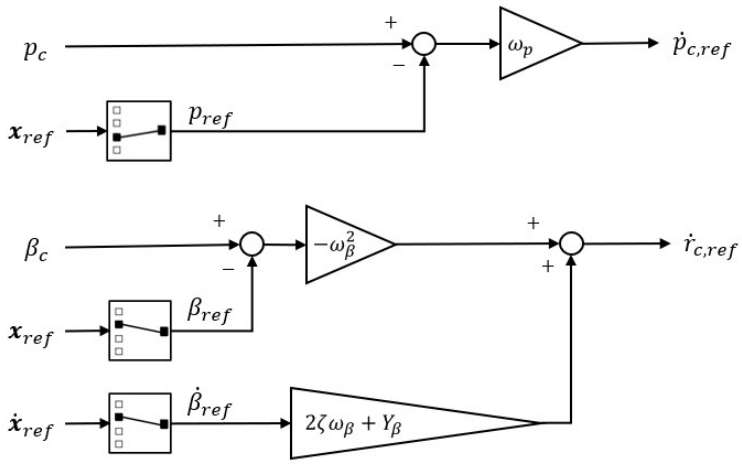

Fig. 2 Decoupled reference model controller

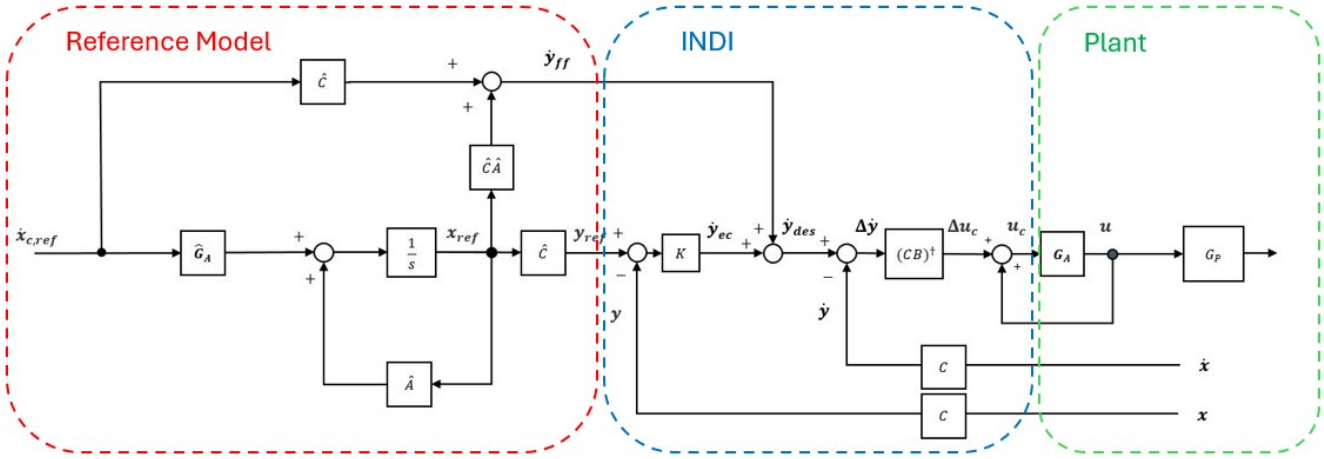

Fig. 3 Vanilla INDI with decoupled dynamic physical reference model

where $\hat{C}$ and $\hat{A}$ are as follows:

$$\hat{A} = \begin{bmatrix} N_r & N_\beta & 0 & 0 \\ -1 & Y_\beta & 0 & 0 \\ 0 & 0 & L_p & 0 \\ 0 & 0 & 1 & 0 \end{bmatrix}, \hat{C} = \begin{bmatrix} 1 & 0 & 0 & 0 \\ 0 & 0 & 1 & 0 \end{bmatrix} \tag{19}$$

Similarly, the reference rate of change of the control variable is formulated as follows:

$$\dot{\boldsymbol{y}}_{ref} = \hat{C}\hat{A}\boldsymbol{x}_{ref} + \hat{C}\hat{G}_A\dot{\boldsymbol{x}}_{c,ref} \tag{20}$$

The closed-loop relation was derived in Eq. (7), and the desired rate of change of the control variable is the same as in Eq. (8). Substituting Eq. (18) and Eq. (8) into Eq. (7) results in:

$$\dot{\boldsymbol{y}} = CA\boldsymbol{x} - G_ACA\boldsymbol{x} + G_A\hat{C}\hat{A}\boldsymbol{x}_{ref} + G_A\hat{C}\dot{\boldsymbol{x}}_{c,ref} + G_AK(\hat{C}\boldsymbol{x}_{ref} - C\boldsymbol{x}) \tag{21}$$

For the nominal case with no disturbance, $\boldsymbol{x}_{ref} = \boldsymbol{x}$, Eq. (21) is simplified to be:

$$\dot{\boldsymbol{y}} = CA\boldsymbol{x} - G_ACA\boldsymbol{x} + G_A\hat{C}\hat{A}\boldsymbol{x}_{ref} + G_A\hat{C}\dot{\boldsymbol{x}}_{c,ref} \tag{22}$$

Since the decoupled plant model differs from the full dynamic model, A and $\hat{A}$ are not equal, which does not result in further simplification. Comparing Eq. (20) and Eq. (22), it is found that:

$$\dot{\boldsymbol{y}} \neq \dot{\boldsymbol{y}}_{ref} \tag{23}$$

which indicates that the feedforward resulting from a reference model with a decoupled plant model cannot, alone, perfectly drive the system to the desired response.

3.3 Performance Evaluation of Reference Model Variants

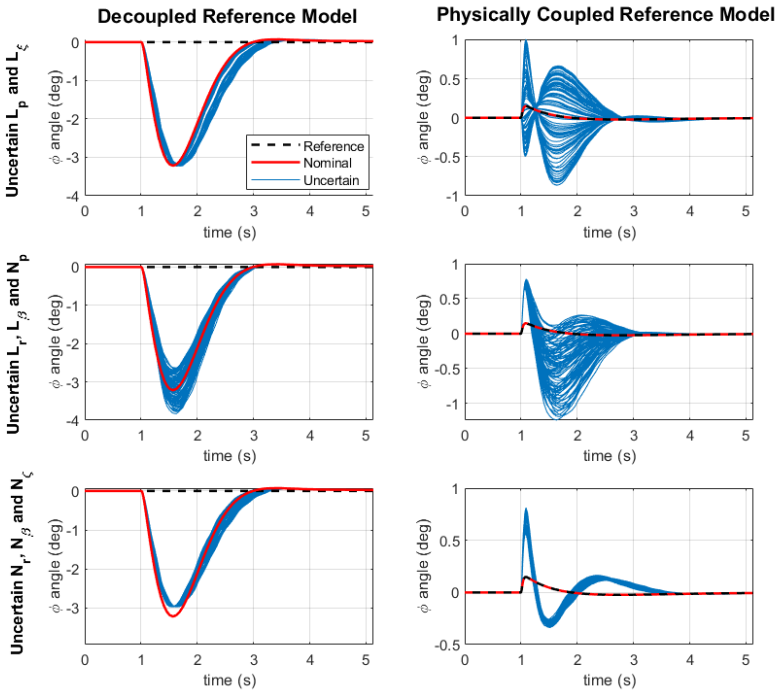

Fig. 4 Comparison of reference model variants under model uncertainty

The physical reference model can be implemented either physically coupled or decoupled. The physically coupled model enables feedforward control, leaving feedback for uncertainties and disturbances. This requires an additional decoupling reference controller, such as DPI, with gain design via eigenstructure assignment and a full coupled model as prerequisites. The decoupled model allows for straightforward design but relies more heavily on the feedback, as it cannot capture cross-channel interactions.

The physically coupled reference model with its controller can achieve perfect decoupling, as we will show in the following under nominal conditions, i.e., upon precise knowledge of the linear plant model. However, the plant model is usually subject to uncertainties. In the following, we therefore investigate the robustness of the two reference model approaches towards uncertainties. A Monte Carlo analysis was conducted to evaluate the effect of various model uncertainties between the reference model plant and the actual plant. One hundred simulations are performed using a step command in the sideslip angle, while maintaining the bank angle at zero, subject to a 20% uncertainty in different model coefficients.

To establish a rate command attitude hold behavior, an integrator is used to transform a roll rate command p_c into the bank angle command ϕ_c for the reference model controller. This command is set to zero for this test. The resulting undesired response in the roll channel was used as a metric for coupling. Across all simulated cases shown in Fig. 4, the physically coupled reference model consistently resulted in lower cross-coupling effects than the decoupled variant.

4 Model-Following iDPI

4.1 Motivation

The iDPI architecture allows for an extension into a model-following structure, where a physical reference model is utilized. Based on this structure, commonly used incremental approaches, such as INDI, are compared with the proposed model-following iDPI framework. The focus of this comparison lies in analyzing the respective error dynamics. In particular, the error dynamics are examined and explicitly utilized for the purpose of gain design. This makes it possible to systematically achieve the desired error dynamics.

4.2 iDPI for Lateral Motion

The filtered Multiple-Input Multiple-Output (MIMO) iDPI controller structure investigated in [11] for lateral motion control is shown in Fig. 5. This proposed controller tracks sideslip angle and bank angle commands. In the block diagram, $G_P(s)$ denotes the plant, and $G_A(s)$ is the diagonal actuator transfer function matrix with identical entries. K_h is a feedforward, K_I an integrator, and K_d a feedback gain matrix.

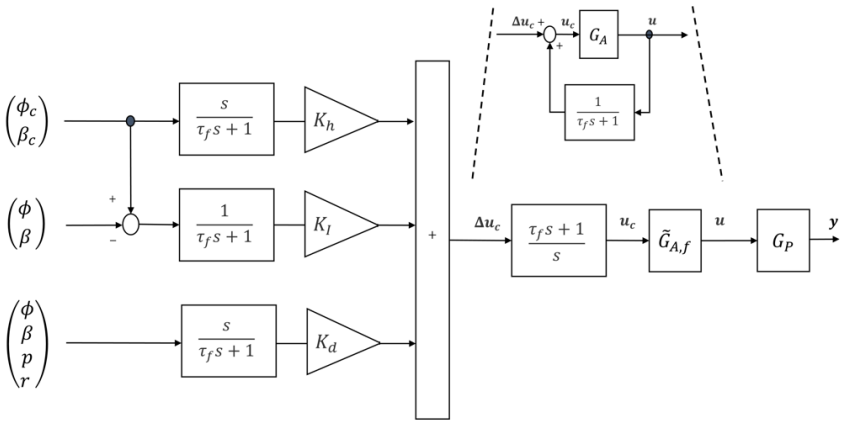

Fig. 5 Filtered iDPI block diagram for lateral motion

A first-order filter is applied to the actuator feedback. For first-order G_A, with time constant τ_a, this is equivalent to $\frac{\tau_f s+1}{s} \cdot \tilde{G}_{A,f}(s)$, where $\tilde{G}_{A,f}(s)$ is diagonal with elements $\tilde{g}_{A,f}(s)$ given by Eq. (24). The filtered equivalent actuator dynamics $\tilde{G}_{A,f}(s)$ are of the same order as the original actuator, but with a lower time constant. The pole of the altered actuator dynamics depends on the time constants of both the filter and the actuator. It is consequently referred to as a shared actuator filter pole.

$$\tilde{g}_{A,f} = \frac{1}{\tau_f + \tau_a} \frac{1}{\left(\frac{\tau_f \tau_a}{\tau_f + \tau_a}\right) s + 1} \tag{24}$$

4.3 Model-Following iDPI for Lateral Motion

A realization of the generic ideal model-following iDPI controller for lateral motion, alongside an ideal standard iDPI, is presented in Fig. 6, where generic control variables, CV_1 and CV_2, are selected for the roll and yaw channels, respectively. It is important to note that this formulation represents an ideal version of iDPI as the integrator arising from the incremental loop is canceled by the derivative applied to the error controller terms. Moreover, in an ideal DPI structure, the integrator would be placed directly before the actuator rather than implemented as an incremental loop around it. However, the incremental

variant of DPI is adopted here, as it has been shown, in [9] and [11], to significantly improve robustness to uncertainties while still preserving the features of the standard DPI approach.

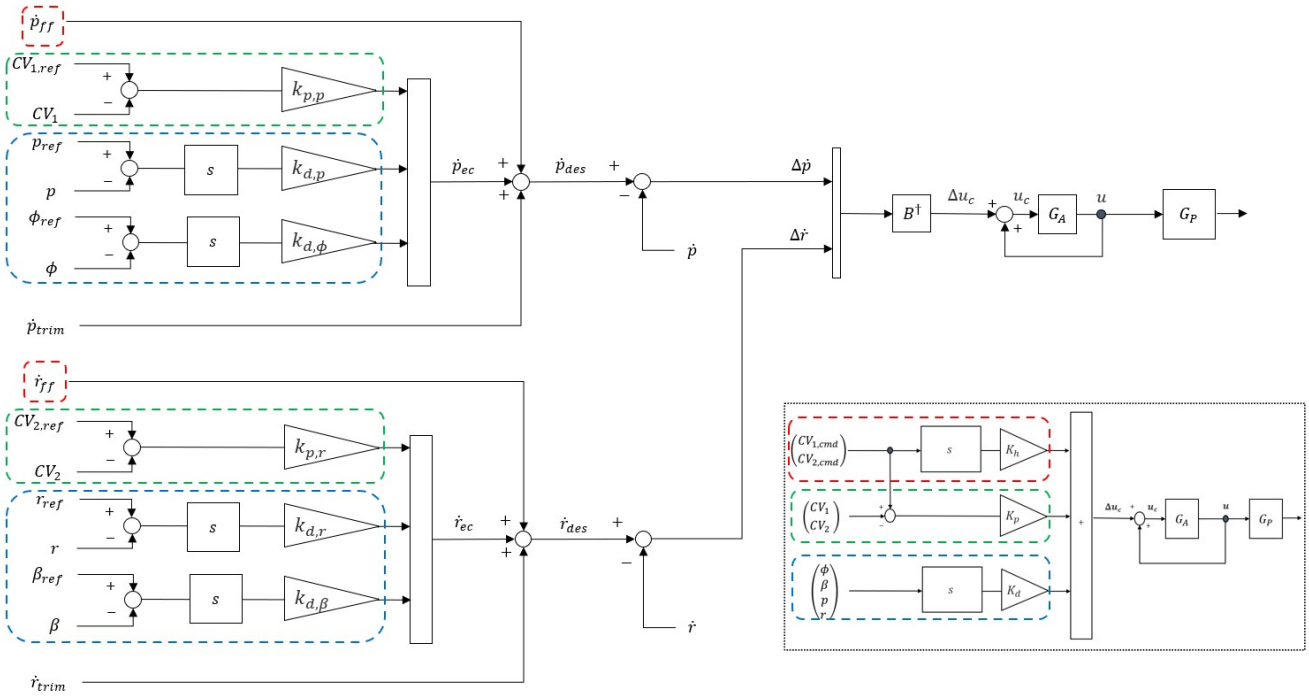

Fig. 6 Generic ideal model-following iDPI control architecture for lateral motion

The following procedure is carried out to derive a model-following iDPI from a standard iDPI, as shown in Fig. 6:

- The roll and yaw channels are divided into two separate loops.
- The feedforward component, marked in red, is replaced by the reference model feedforward.
- The control variables error terms, marked in green, are calculated with respect to the reference variables instead of the command.
- The feedback terms, marked in blue, are chosen as errors from the reference variables rather than the full states. This ensures that only deviations from the reference values are damped.
- $\dot{p}_{trim}$ and $\dot{r}_{trim}$ are added in order to maintain steady-state flight in the absence of control inputs and account for the coupling effect between both channels if required.
- Δu is computed by mapping the errors in roll and yaw angular accelerations $(\Delta\dot{p}, \Delta\dot{r})$ through the inverse of the control effectiveness represented by B matrix.

4.4 Error Controller Structure

The error controller generates the desired roll and yaw accelerations, each composed of three components: a feedforward component based on the reference model dynamics, an error correction term based on the feedback signals, and trim values needed to maintain steady-state flight in the absence of control inputs. This is written as follows:

$$\begin{aligned} \dot{p}_{des} &= \dot{p}_{ec} + \dot{p}_{ref} + \dot{p}_{trim} \\ \dot{r}_{des} &= \dot{r}_{ec} + \dot{r}_{ref} + \dot{r}_{trim} \end{aligned} \tag{25}$$

The incremental loop ensures that $\dot{p}$ and $\dot{r}$ track $\dot{r}_{des}$ and $\dot{p}_{des}$, respectively. We assume that modeling errors or disturbances lead to a deviation:

$$\begin{aligned} \dot{p} &= \dot{p}_{des} - \delta_{\dot{p}} \\ \dot{r} &= \dot{r}_{des} - \delta_{\dot{r}} \end{aligned} \tag{26}$$

In the following, we derive the error dynamics associated with the controller structure presented in Fig. 6.

4.4.1 Roll Channel

The roll channel control variable is chosen to be the roll rate p, i.e., operates on a roll rate command/roll rate control basis (p_{cmd}/p_{ctrl}). The output of the controller to the incremental loop and control allocation is the desired roll acceleration:

$$\dot{p}_{des} = \dot{p}_{ref} + \dot{p}_{trim} + \dot{p}_{ec} = \dot{p} + \delta_{\dot{p}} \tag{27}$$

The error controller, $\dot{p}_{ec}$, for the model-following iDPI is written as follows:

$$\dot{p}_{ec} = k_{p,p}(p_{ref} - p) + k_{d,p}s(p_{ref} - p) + k_{d,\phi}s(\phi_{ref} - \phi) \tag{28}$$

Substituting Eq. (28) into Eq. (27) results in:

$$\dot{p}_{ref} + \dot{p}_{trim} + k_{p,p}(p_{ref} - p) + k_{d,p}s(p_{ref} - p) + k_{d,\phi}s(\phi_{ref} - \phi) = \dot{p} + \delta_{\dot{p}} \tag{29}$$

Rewriting the above equation and omitting the trim term:

$$\dot{e}_p + k_{p,p}e_p + k_{d,p}\dot{e}_p + k_{d,\phi}e_p = \delta_{\dot{p}} \tag{30}$$

where the error terms are:

$$\begin{aligned} \dot{e}_p &= \dot{p}_{ref} - \dot{p} \\ e_p &= p_{ref} - p \end{aligned} \tag{31}$$

Further simplifying the above equation yields Eq. (32), which exhibits first-order dynamics of the roll rate and a disturbance $\delta\dot{p}$ that would excite the dynamics . The controller parameters enable the independent shaping of the first-order dynamics, i.e., the time constant, and disturbance rejection by increasing $k_{d,p}$. The controller architecture for p_{cmd}/p_{ctrl} is shown in Fig. 7.

$$\dot{e}_p + \frac{k_{p,p} + k_{d,\phi}}{1 + k_{d,p}}e_p = \frac{1}{1 + k_{d,p}}\delta_{\dot{p}} \tag{32}$$

4.4.2 Yaw Channel

The yaw channel control variable is chosen to be the sideslip angle β, i.e., operates on a sideslip command/yaw rate control basis (β_{cmd}/r_{ctrl}). The yaw channel is different than the roll channel in the sense that for the roll channel, the control variable is the roll rate, which has a relative degree one dynamics. Consequently, the error dynamics in the roll channel are relatively straightforward. Conversely, the yaw channel's control variable is the sideslip angle, characterized by relative degree two dynamics. Because the sideslip angle is regulated via the yaw rate, it necessitates linking the sideslip dynamics with the yaw rate dynamics to derive the resultant sideslip error dynamics.

The output of the controller to the incremental loop and the control allocation is a desired yaw acceleration, which is represented as follows:

$$\dot{r}_{des} = \dot{r}_{ref} + \dot{r}_{trim} + \dot{r}_{ec} = \dot{r} + \delta_{\dot{r}} \tag{33}$$

By differentiating the $\dot{\beta}$ equation in Eq. (1), and solving for $\dot{r}$, the yaw acceleration with only lateral gust disturbance is derived to be equal to:

$$\dot{r} = -\ddot{\beta} + Y_\beta \dot{\beta} + \frac{g}{V_0}\dot{\phi} - \frac{Y_\beta}{V_0}\dot{v}_g \tag{34}$$

where Y_ξ,Y_ζ, Y_r and Y_p were neglected due to their low magnitude.

In case the full coupled dynamic reference model is utilized, the reference yaw acceleration is equal to:

$$\dot{r}_{ref} = -\ddot{\beta}_{ref} + \hat{Y}_\beta \dot{\beta}_{ref} + \frac{g}{V_0}\dot{\phi}_{ref} \tag{35}$$

where $\hat{Y}_\beta$ represents the assumed stability derivative Y_β.

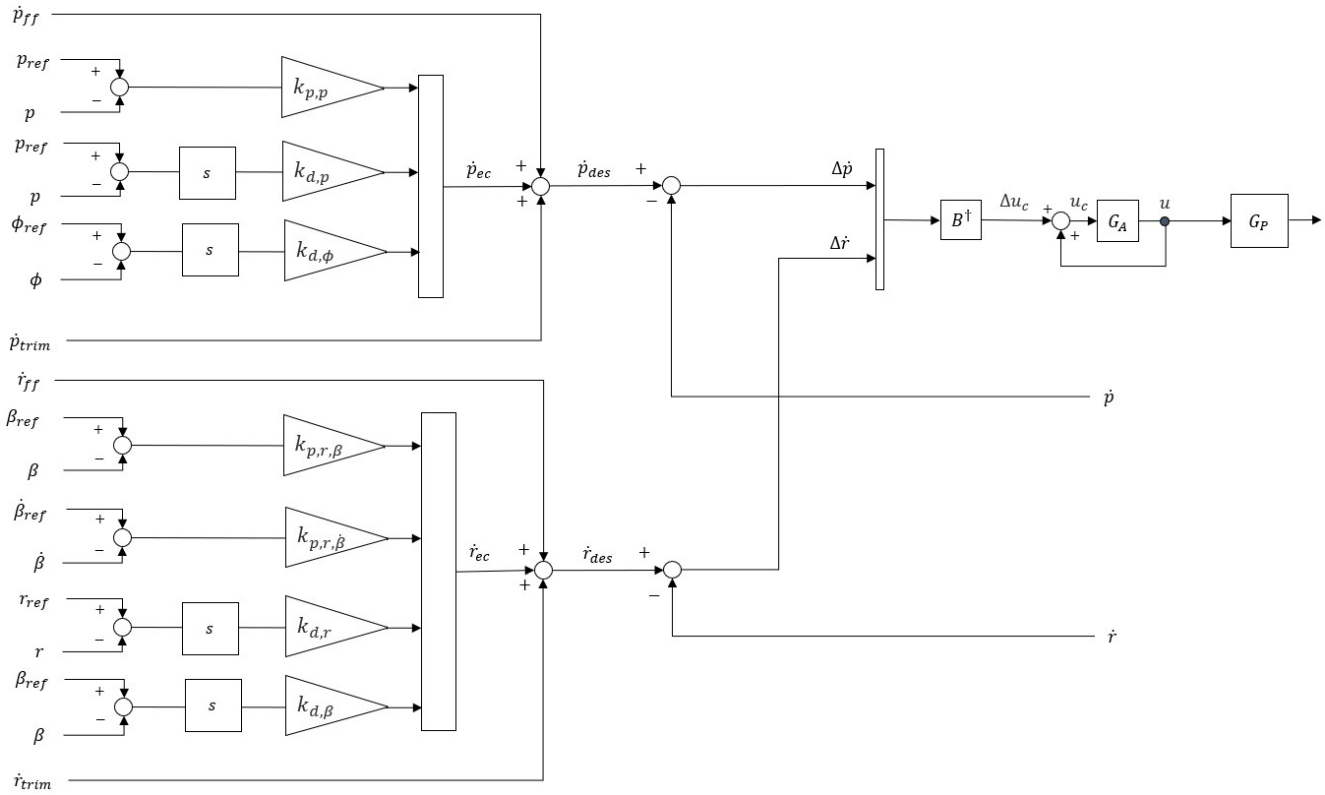

Fig. 7 Ideal model-following iDPI control architecture with p_{cmd}/p_{ctrl} and β_{cmd}/r_{ctrl}

Since the sideslip angle is regulated through the yaw rate, the yaw rate dynamics are expressed in terms of the sideslip. This formulation yields a second-order dynamic representation of the sideslip angle, which can be shaped using the feedback gains $k_{p,r,\beta}$ and $k_{p,r,\dot{\beta}}$ acting on the error of the sideslip angle and the rate of change, respectively. This is reflected in $\dot{r}_{ec}$ expression in Eq. (36), and represented in the control structure shown in Fig. 7.

$$\dot{r}_{ec} = -k_{p,r,\beta}(\beta_{ref} - \beta) - k_{p,r,\dot{\beta}}(\dot{\beta}_{ref} - \dot{\beta}) + k_{d,\beta}s(\beta_{ref} - \beta) + k_{d,r}s(r_{ref} - r) \tag{36}$$

Inserting Eq. (36) into Eq. (33) and re-writing the equation yields:

$$(1 + k_{d,r})\dot{e}_r + \dot{r}_{trim} - k_{p,r,\beta}e_\beta + (k_{d,\beta} - k_{p,r,\dot{\beta}})\dot{e}_\beta = \delta_{\dot{r}} \tag{37}$$

where

$$\begin{aligned} \dot{e}_\beta &= \dot{\beta}_{ref} - \dot{\beta} \\ e_\beta &= \beta_{ref} - \beta \\ \dot{e}_r &= \dot{r}_{ref} - \dot{r} \end{aligned} \tag{38}$$

Since a full dynamic reference model will be utilized for the iDPI, substitute Eq. (34) and Eq. (35) into Eq. (37):

$$(1 + k_{d,r})(-\ddot{e}_\beta + \hat{Y}_\beta\dot{\beta}_{ref} - Y_\beta\dot{\beta} + \frac{g}{V_0}\dot{e}_\phi + \frac{Y_\beta}{V_0}\dot{v}_g) + \dot{r}_{trim} - k_{p,r,\beta}e_\beta + (k_{d,\beta} - k_{p,r,\dot{\beta}})\dot{e}_\beta = \delta_{\dot{r}} \tag{39}$$

The trim term is selected to remove the coupling effect as follows:

$$\dot{r}_{trim} = -\frac{g(1 + k_{d,r})}{V_0}\dot{e}_\phi \tag{40}$$

Applying Eq. (40) into Eq. (39) and further simplifying the equation results in:

$$-\ddot{e}_\beta + (\hat{Y}_\beta + \frac{k_{d,\beta} - k_{p,r,\dot{\beta}}}{1 + k_{d,r}})\dot{e}_\beta - \frac{k_{p,r,\beta}}{1 + k_{d,r}}e_\beta = \frac{\delta_{\dot{r}}}{1 + k_{d,r}} - \frac{Y_\beta}{V_0}\dot{v}_g - (\hat{Y}_\beta - Y_\beta)\dot{\beta} \tag{41}$$

It is observed in Eq. (41) that the sideslip angle follows a second-order dynamics that can be shaped through the controller parameters. The disturbance and model-mismatch terms act as excitations of this dynamics, and certain contributions can be attenuated by increasing $k_{d,r}$.

4.5 Comparison with INDI

Model-following INDI follows the same exact error dynamics derivation. However, the error controller looks different. In the INDI error controller the following gains in Eq. (32) and Eq. (41) are zero:

$$k_{d,p} = k_{d,\phi} = k_{d,r} = k_{d,\beta} = 0 \tag{42}$$

Table 1 presents the final error dynamics for INDI and iDPI controllers in both the roll and yaw channels. It is visible that the iDPI controller has more parameters and degrees of freedom. In the nominal case, where the model is fully known, and no disturbances affect the system, for both the INDI and iDPI, the parameters can be selected such that they exhibit identical error dynamics with the correct trim being utilized in each controller. Although the iDPI controller offers more degrees of freedom and additional gains to shape the dynamics, these gains are redundant and unnecessary. The primary difference between the two controllers becomes evident when examining the error dynamics in off-nominal cases.

Table 1 Error dynamics for Model-Following INDI and iDPI

	INDI	**iDPI**
$\boldsymbol{p_{cmd}/p_{ctrl}}$	$\dot{e}_p + k_{p,p}e_p = \delta_{\dot{p}}$	$\dot{e}_p + \frac{k_{p,p}+k_{d,\phi}}{1+k_{d,p}}e_p = \frac{1}{1+k_{d,p}}\delta_{\dot{p}}$
$\boldsymbol{\beta_{cmd}/r_{ctrl}}$	$-\ddot{e}_\beta + (\hat{Y}_\beta - k_{p,r,\dot{\beta}})\dot{e}_\beta - k_{p,r,\beta}e_\beta$ $= \delta_{\dot{r}} - \frac{Y_\beta}{V_0}\dot{v}_g - (\hat{Y}_\beta - Y_\beta)\dot{\beta}$	$-\ddot{e}_\beta + (\hat{Y}_\beta + \frac{k_{d,\beta}-k_{p,r,\dot{\beta}}}{1+k_{d,r}})\dot{e}_\beta - \frac{k_{p,r,\beta}}{1+k_{d,r}}e_\beta +$ $= \frac{1}{1+k_{d,r}}\delta_{\dot{r}} - \frac{Y_\beta}{V_0}\dot{v}_g - (\hat{Y}_\beta - Y_\beta)\dot{\beta}$

For the off-nominal cases, the iDPI provides the additional gains $k_{d,p}$ and $k_{d,r}$ that allow to effectively reduce the effect of disturbances on the error dynamics which is represented above by $\delta_{\dot{p}}$ and $\delta_{\dot{r}}$. In addition, the desired overall error dynamic behavior can still be preserved through the adjustment of other gains, in particular $k_{p,p}$ and $k_{p,r,\dot{\beta}}$ and $k_{p,r,\beta}$. The other gains introduced by the iDPI methodology, in this case $k_{d,\phi}$ and $k_{d,\beta}$, are unnecessary as they do not introduce any new degrees of freedom for the design and can be omitted in order to reduce the overall system complexity.

In order to validate the above error dynamics and the additional benefits introduced by the iDPI controller architecture, a physically coupled reference model is utilized, and the overall error dynamics is chosen to be equal to the following dynamics:

$$\begin{aligned} \omega_p &= 3 \ rad/s \\ \omega_\beta = 3 \ rad/s, \quad \zeta_\beta &= 0.7 \end{aligned} \tag{43}$$

The INDI and iDPI controller gains are selected in order to achieve the overall error dynamics specified by Eq. (43). Since it was proven in Section 3.2 that utilizing a full dynamic model allows the feedforward alone to achieve perfect tracking, the error signals are all zero, and hence the error controller output is also zero. Therefore, a lateral gust disturbance is applied, and the feedforward term is omitted by giving zero commands to facilitate checking the error dynamics of each controller.

The lateral gust disturbance is represented by a discrete gust model with a 1 - cos shape, which follows the discrete gust design criterion mentioned in [14], where $V_{g,\mathrm{d}}$ represents the design gust velocity and H is the gust gradient distance. For this investigation, a design gust velocity of $15m/s$ and a gust gradient distance of $1.5m$ is selected.

$$V_g = \begin{cases} \frac{V_{g,\mathrm{d}}}{2}\left[1 - \cos\left(\frac{\pi t}{H}\right)\right] & 0 \le t \le 2H \\ 0 & t > 2H \end{cases} \tag{44}$$

Fig. 8 shows the roll rate and sideslip angle response to a lateral gust disturbance. To demonstrate the impact of additional gains that mitigate disturbance effects in the iDPI architecture, as indicated in Table 1, different magnitudes of $k_{d,p}$ and $k_{d,r}$ are applied, as shown in Table 2. At zero magnitude, both INDI and iDPI are identical, as setting these gains to zero results in both controllers having the same error dynamics, making them equally affected by the disturbance. As the gains increase, the roll rate and sideslip angle perturbation due to the lateral gust disturbance decrease, as expected from the overall error dynamics of iDPI.

Table 2 Error controller gain sets

Gain sets	**Roll Channel**	**Yaw Channel**
INDI	$k_{p,p} = 3.00$	$k_{p,r,\beta} = 9.00, k_{p,r,\dot{\beta}} = 4.38,$
iDPI: gain set 0	$k_{p,p} = 3.00, k_{d,\phi} = 0.0, k_{d,p} = 0.00$	$k_{p,r,\beta} = 9.00, k_{p,r,\dot{\beta}} = 4.38, k_{d,\beta} = 0.0, k_{d,r} = 0.00$
iDPI: gain set 1	$k_{p,p} = 3.75, k_{d,\phi} = 0.0, k_{d,p} = 0.25$	$k_{p,r,\beta} = 11.3, k_{p,r,\dot{\beta}} = 5.46, k_{d,\beta} = 0.0, k_{d,r} = 0.25$
iDPI: gain set 2	$k_{p,p} = 4.50, k_{d,\phi} = 0.0, k_{d,p} = 0.50$	$k_{p,r,\beta} = 13.5, k_{p,r,\dot{\beta}} = 6.55, k_{d,\beta} = 0.0, k_{d,r} = 0.50$

To assess the impact of higher gain settings on stability margins, the gain and phase margins, along with the phase margin frequency, are presented in Table 3. For the roll axis actuator cut, $u_{c,\xi}$, both gain and phase margins are higher for the INDI and iDPI with gain set 0, but these margins decrease as the gain increases. Conversely, for the yaw axis actuator cut, $u_{c,\zeta}$, the margins improve as the gain increases. This also holds for $\Delta u_{c,\xi}$ and $\Delta u_{c,\zeta}$. However, this improvement comes with the side effect of an increase in the phase margin frequency, which should be considered while choosing suitable gains. Regarding the

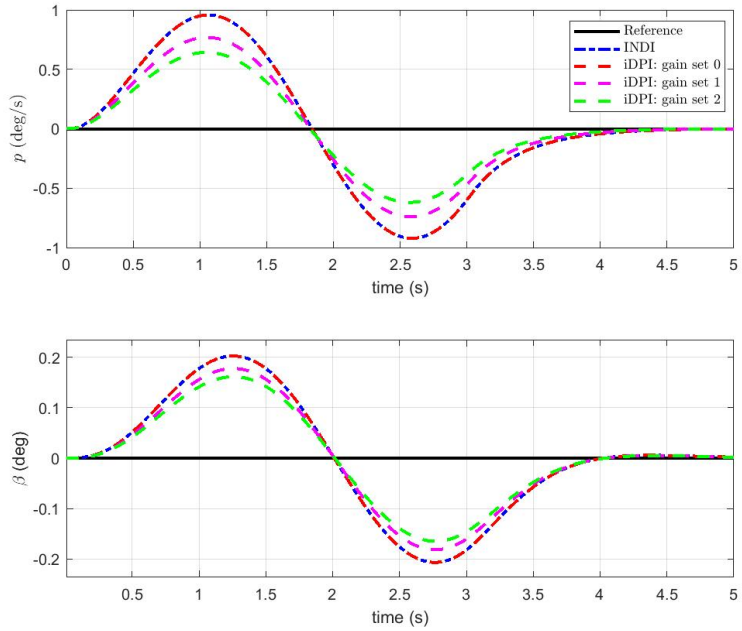

Fig. 8 Roll rate and sideslip angle under lateral gust disturbance with different gain sets

Table 3 Gain margin and Phase margin (frequency) at different loop cuts

	INDI/ iDPI: gain set 0	**iDPI: gain set 1**	**iDPI: gain set 2**
$u_{c,\xi}$	$18.7dB/104°\ (0.02\,rad/s)$	$12.9dB/84.7°\ (0.03\,rad/s)$	$3.6dB/62.4°\ (0.04\,rad/s)$
$u_{c,\zeta}$	$\infty/85.7°\ (4.7\,rad/s)$	$\infty/100.8°\ (5.7\,rad/s)$	$\infty/117.5°\ (7.5\,rad/s)$
$\Delta u_{c,\xi}$	$\infty/76.3°\ (24.9\,rad/s)$	$\infty/81.3°\ (30.6\,rad/s)$	$\infty/86.1°\ (36.8\,rad/s)$
$\Delta u_{c,\zeta}$	$\infty/70.2°\ (27.6\,rad/s)$	$\infty/77.0°\ (33.8\,rad/s)$	$\infty/83.1°\ (40.9\,rad/s)$
r	$\infty/82.3°\ (4.0\,rad/s)$	$\infty/83.7°\ (4.1\,rad/s)$	$\infty/84.7°\ (4.1\,rad/s)$
β	$\infty/89.9°\ (0.23\,rad/s)$	$\infty/89.9°\ (0.23\,rad/s)$	$\infty/89.9°\ (0.23\,rad/s)$
p	$\infty/89.9°\ (3.0\,rad/s)$	$\infty/89.9°\ (3.0\,rad/s)$	$\infty/89.9°\ (3.0\,rad/s)$
ϕ	∞/∞	∞/∞	∞/∞

sensor cuts, the data show that their margins remain consistent across different gain settings, indicating that they are not significantly influenced by changes in the gain.

5 Application to High-Fidelity Nonlinear Flight Dynamic Model of a Commercial Aircraft

The concept of model-following iDPI was applied to control the lateral motion of the DO-728 aircraft. To enable real-world implementation, several practical adaptations were required. Before we detail the adaptations made for our application specifically, we first summarize the key aspects that may be generally considered in this context.

- **Filtered iDPI:** The ideal iDPI is typically not feasible to implement in practice because of the direct differentiation represented by the Laplace operator s as can be seen in Fig. 6. Instead, filtering can be applied as shown in Fig. 5 or in Fig. 9 where the filtering is represented by $L(s)$. The derivative filters $L(s)$ before the controller gains cancel with the virtual integrator filter after the

control gains (which results from the incremental actuator feedback loop) in the fixed gain linear analysis, and remove the hidden coupling terms when analyzing the gain-scheduled controller, as proven in [9]. Note: In contrast to Fig. 5, we do not apply the filter $L(s)$ in the actuator feedback in Fig. 9 because it is incorporated in the hybrid complementary filter as will be detailed later.

- **Sideslip Rate Estimation:** The measurement of β is often noisy or unavailable. Differentiation, even when filtered as suggested by the filtered iDPI, could amplify the noise to an unacceptable level. In this case, as proposed by [10], the sideslip angle rate can be estimated from the lateral load factor using the kinematic relationship:

$$\hat{\dot{\beta}}_A = \frac{g}{\left(V_A^G\right)^E}\left(\left(n_y\right)_B + \cos\theta \sin\phi\right) - r_K \tag{45}$$

- **Control allocation:** In over-actuated systems, control allocation algorithms can distribute the commanded rate accelerations to the available control effectors while considering actuator limits and rate constraints. Two widely used approaches are the Redistributed Pseudo-Inverse (RSPI) [15], and the ERP [16] methods. When the commanded pseudo-control cannot be achieved with the available effector limits, these allocation schemes scale the commands such that the desired pseudo-control direction is preserved. It has been shown in [17] that RSPI and ERP lead to equivalent results. Further work has extended RSPI to include null-space transitions, enabling smooth redistribution of commands when actuators reach their limits, and expanded it specifically for usage in the context of safety-critical applications [18].

- **Additional Signal Processing and Filtering:** In real-world applications, measurements are usually filtered with roll-off or notch filters, are delayed, or include sensor dynamics. These effects are represented in Fig. 9 with $F(s)$.

- **Synchronized Angular Acceleration Complementary Estimation Filter:** The model-following iDPI architecture requires roll and yaw acceleration signals. It is often not possible to measure the angular accelerations directly; thus, an estimation filter is required. As [19] shows, incremental loops in combination with angular acceleration filters and additional signal filtering require careful synchronization.

5.1 Control Variables and Controller Structure

The control variables are selected such that the pilot commands roll rate p_c and lateral load factor $n_{y,c}$. The lateral load factor was chosen in the directional channel due to the unavailability of a sideslip measurement. The steady state sideslip error can be estimated using the lateral load factor error information, to output the following relation [10]:

$$e_{\hat{\beta}} = \frac{g}{Y_\beta V} e_{n_y} \tag{46}$$

In order to create a rate command attitude hold behavior, a prefilter is used to transform a roll rate command p_c into the bank angle command for the reference model controller. This prefilter is designed with a desired first-order dynamics with the time constant τ_s as shown in Eq. (47).

$$\phi_c = \frac{(\tau_s s + 1)}{s} p_c \tag{47}$$

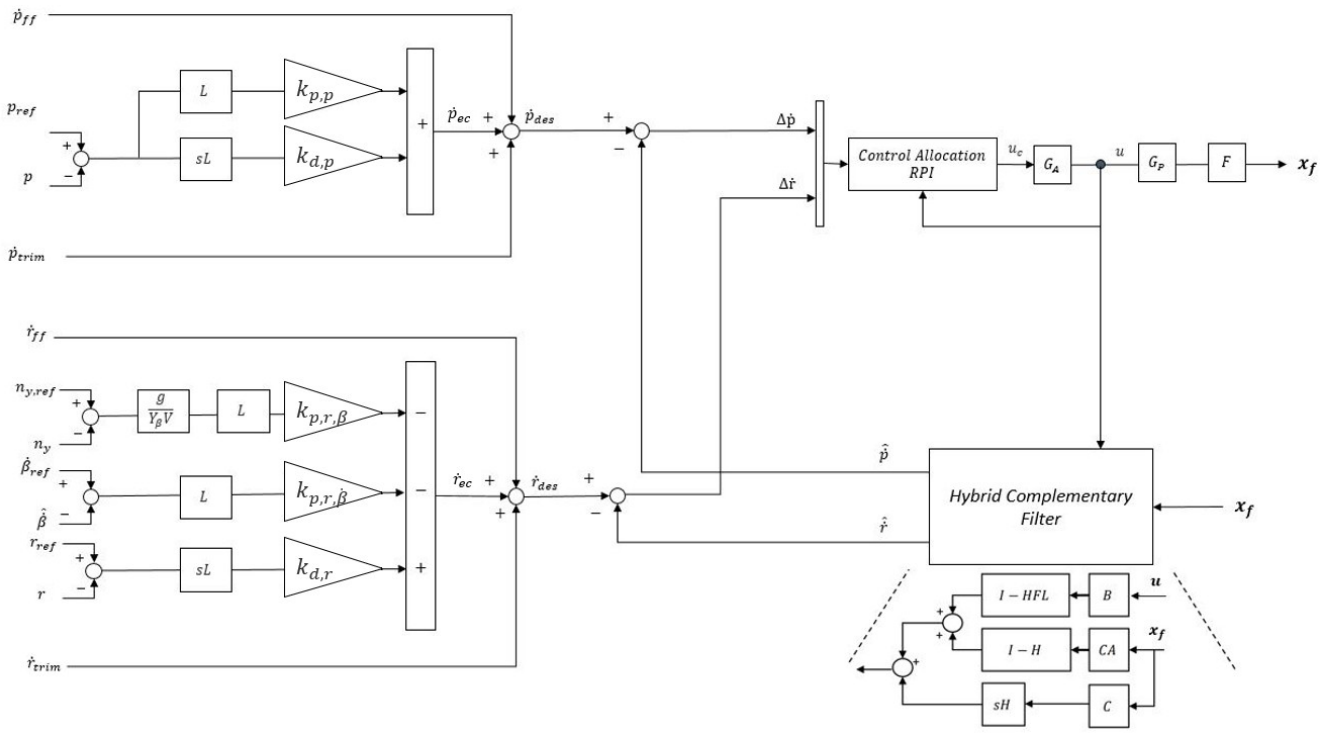

Fig. 9 Lateral iDPI controller architecture with Hybrid Complementary Filter

The model-following variant is utilized in combination with the physically coupled dynamic physical reference model, presented in Section 3.2.1. The complete lateral iDPI controller structure with the discussed control variables, hybrid complementary filter, control allocation, and filters can be seen in Fig. 9. The final iDPI error controller is based on the findings in 4.5. Within the architecture, the filter denoted as L represents a low-pass filter expressed as $L(s) = \frac{1}{\tau s+1}$ with time constant τ, and F comprises additional dynamics of the measurements, like roll-off filtering.

5.2 Estimations

Angular Acceleration Estimation: It is often not possible to measure the angular accelerations directly; thus, an estimation filter is required. The hybrid complementary filter was first introduced in [20], and then reformulated in [21], which is used for this purpose. It takes into account and synchronizes for the dynamics and delays introduced by $L(s)$ and $F(s)$. Furthermore, it accounts for system dynamics via a model-based estimate of the angular accelerations, as the state contributions had a noticeable impact. The structure of the hybrid complementary filter that is utilized in this study is shown in Fig. 9.

Sideslip Angle Rate: The rate of change of the sideslip angle $\hat{\dot{\beta}}$ is obtained using Eq. (45).

6 Simulation Results

The proposed controller was integrated into the nonlinear six-degree-of-freedom model of the DO 728 and evaluated at a representative trimmed flight condition corresponding to a single point in the flight envelope. Figures 10 and 11 present the responses to roll rate and lateral load factor doublet commands, respectively, together with the commands and the reference model output. The figures also include the state evolution and surface deflections predicted by the reference model, labeled as *design*.

For the roll rate command in Fig. 10, the measured roll rate closely follows the reference response with negligible steady state error and well-damped transients. The rise time and overshoot are consistent with the reference model dynamics, indicating that the model-following objective is achieved. The sideslip

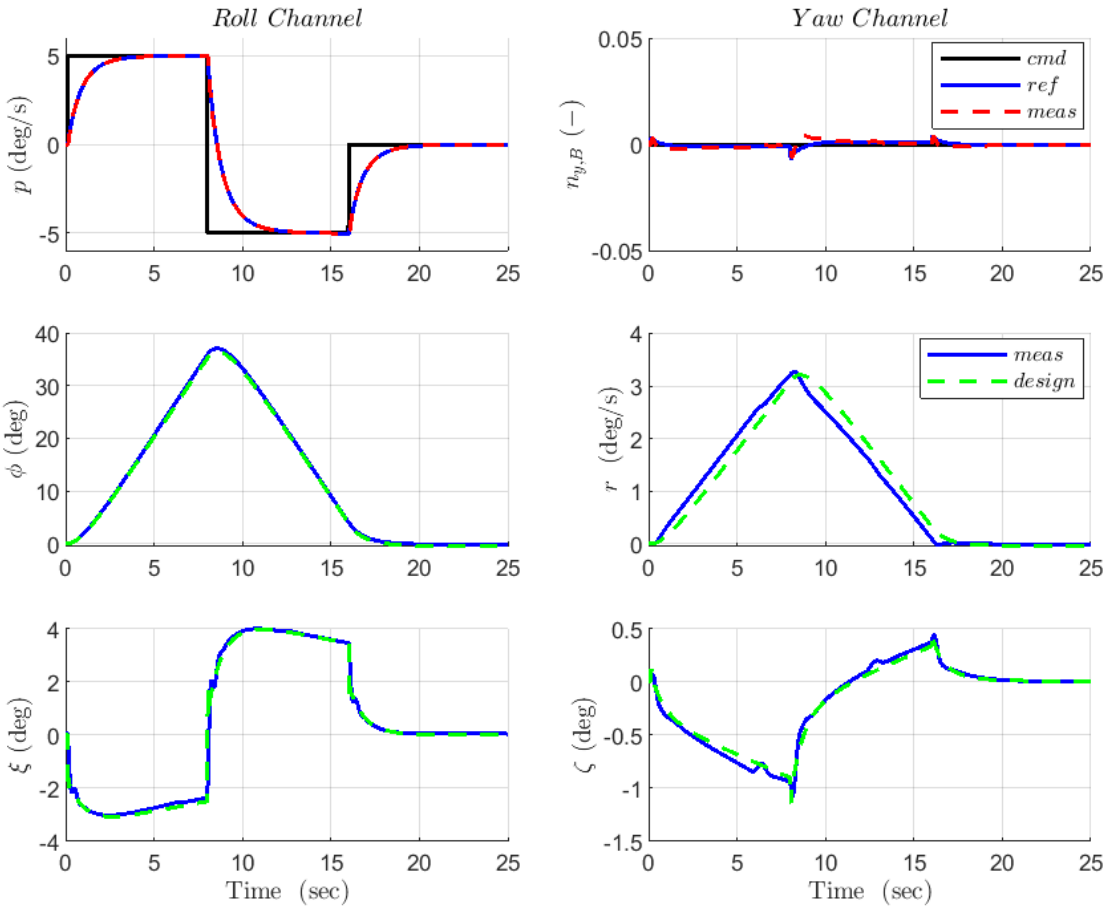

Fig. 10 Simulation results with predicted and actual response for a roll rate doublet command

response remains close to zero throughout the maneuver, demonstrating effective decoupling between the roll and yaw channels. The corresponding aileron and rudder deflections remain smooth and bounded, with no excessive control activity.

For the lateral load factor command in Fig. 11, accurate tracking is again observed. The induced roll rate response is consistent with coordinated motion and matches the predicted reference dynamics, confirming that the reference model correctly captures the coupled behavior. The control surface deflections exhibit physically consistent trends and remain within reasonable limits.

In both cases, the state trajectories and actuator responses closely match the nonlinear simulation results, validating the consistency between the linear physical reference model and the full nonlinear plant. The small discrepancies observed during sharp transients can be attributed to nonlinear effects and unmodeled dynamics, yet they do not influence overall tracking or stability. Overall, the results demonstrate that the proposed model-following iDPI structure achieves accurate tracking of the desired closed-loop dynamics while maintaining effective channel decoupling and realistic control effort at the evaluated flight condition.

7 Conclusions

This work develops a model-following iDPI framework that extends the traditional iDPI concept to systematically decouple desired closed-loop behavior from disturbance rejection and robustness in MIMO flight control systems. This separation allows the feedforward path to drive the ideal system

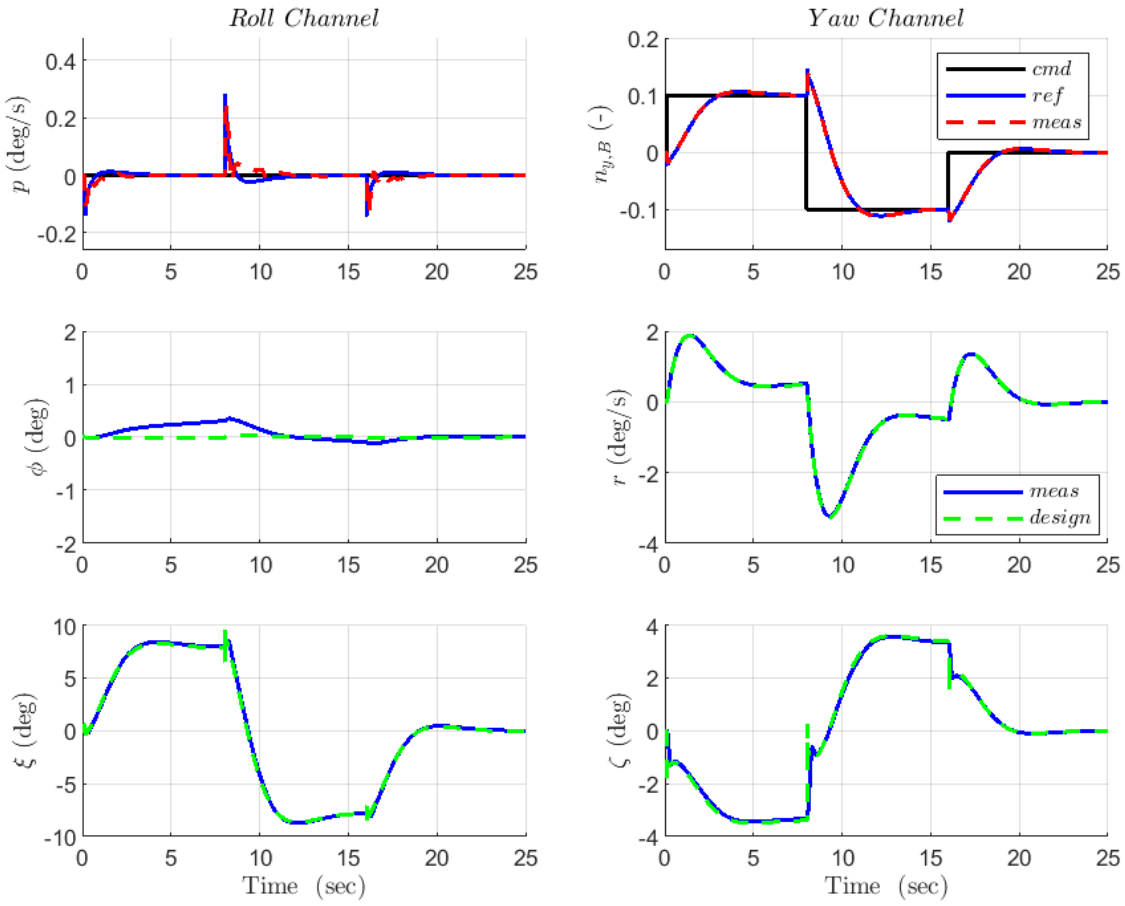

Fig. 11 Simulation results with predicted and actual response for a lateral load factor doublet command

behavior while the error controller is reserved exclusively for managing external disturbances and model uncertainties.

Analytical analysis of different variants of reference models demonstrates that the physically coupled reference model outperforms simplified decoupled variants by preserving essential channel interactions, thereby mitigating cross-coupling effects and reducing feedback activity during tracking. Furthermore, the investigation into error dynamics confirms that the iDPI framework offers practical advantages over standard INDI. The introduction of additional derivative gains provides more degrees of freedom to independently shape the error dynamics and effectively attenuate disturbances.

High-fidelity simulation results further validate the proposed approach, demonstrating its effectiveness in achieving satisfactory performance in modern aircraft configurations. These results highlight the potential of such framework as a systematic and implementable methodology for advanced flight control design. Future work will focus on extending the model-following iDPI structure to accommodate longitudinal motion, investigating performance across the full flight envelope, and conducting experimental flight tests to comprehensively assess and validate the architecture under real-world operational conditions.

Declaration of Use of Artificial Intelligence

Artificial intelligence was not used in the work presented.

References

[1] Stefan A. Raab, Jiannan Zhang, Pranav Bhardwaj, and Florian Holzapfel. *Consideration of Control Effector Dynamics and Saturations in an Extended INDI Approach*. 2019. ISBN: 9781510893122. doi: 10.2514/6.2019-3267.

[2] Rasmus Steffensen, Agnes Steinert, and Ewoud J. J. Smeur. Nonlinear dynamic inversion with actuator dynamics: An incremental control perspective. *Journal of Guidance, Control, and Dynamics*, 46(4):709–717, 2023. doi: 10.2514/1.G007079.

[3] Yue Liu, Agnes Steinert, Haichao Hong, Hangxu Li, and Shiqiang Hu. Nonlinear dynamic inversion with generalized actuator dynamics: Performance and stability. *Aerospace Science and Technology*, 162:110218, 2025. ISSN: 1270-9638. doi: https://doi.org/10.1016/j.ast.2025.110218.

[4] Tomaso Ponti, Simon Hafner, Ewoud Smeur, and Bart Remes. Actuator nonlinear dynamic inversion for systems with heterogeneous actuator dynamics: A superior alternative to incremental nonlinear dynamic inversion, 01 2025. doi: 10.2139/ssrn.5399001.

[5] Agnes STEINERT, Stefan RAAB, Simon HAFNER, Florian HOLZAPFEL, and Haichao HONG. From fundamentals to applications of incremental nonlinear dynamic inversion: A survey on indi – part i. *Chinese Journal of Aeronautics*, page 103553, 2025. ISSN: 1000-9361. doi: https://doi.org/10.1016/j.cja.2025.103553.

[6] Agnes STEINERT, Stefan RAAB, Simon HAFNER, Florian HOLZAPFEL, and Haichao HONG. Advancements in incremental nonlinear dynamic inversion and its components: A survey on indi – part ii. *Chinese Journal of Aeronautics*, page 103591, 2025. ISSN: 1000-9361. doi: https://doi.org/10.1016/j.cja.2025.103591.

[7] Wilson J. Rugh and Jeff S. Shamma. Research on gain scheduling. *Automatica*, 36(10):1401–1425, 2000. ISSN: 0005-1098. doi: https://doi.org/10.1016/S0005-1098(00)00058-3.

[8] Robert Osterhuber, Martin Hanel, and Rainer Hammon. Realization of the eurofighter 2000 primary lateral/directional flight control laws with differential pi-algorithm. 08 2004. ISBN: 978-1-62410-073-4. doi: 10.2514/6.2004-4751.

[9] Rasmus Steffensen, Agnes Steinert, and Florian Holzapfel. Incremental control as an enhanced and robust implementation of gain scheduled controllers avoiding hidden coupling terms. *Aerospace Science and Technology*, 141:108500, 2023. ISSN: 1270-9638. doi: https://doi.org/10.1016/j.ast.2023.108500.

[10] Rasmus Steffensen, Kilian Ginnell, and Florian Holzapfel. Practical system identification and incremental control design for a subscale fixed-wing aircraft. *Actuators*, 13(4), 2024. ISSN: 2076-0825. doi: 10.3390/act13040130.

[11] Marwan Shalaby, Agnes Steinert, David Basta, and Florian Holzapfel. Incremental differential proportional-integral control (iDPI) for MIMO fixed-wing aircraft dynamics. Manuscript submitted for publication to Mediterranean Conference on Control and Automation (MED), 3 2026.

[12] Fubiao Zhang, Stanislav Braun, and Florian Holzapfel. *Physically Integrated Reference Model and Its Aids in Model Based Flight Control Development*. 2014. ISBN: 9781632669322. doi: 10.2514/6.2014-0962.

[13] Agnes Steinert, Rasmus Steffensen, Rafael De Angelis Cordeiro, José Azinheira, Alexandra Moutinho, and Florian Holzapfel. Integration of phase plane flight envelope protections in cascaded incremental flight control. *IFAC-PapersOnLine*, 52:429–435, 01 2019. doi: 10.1016/j.ifacol.2019.11.281.

[14] Federal Aviation Administration. Airworthiness standards: Transport category airplanes. Technical report, Federal Aviation Administration, 2020. `https://www.ecfr.gov/current/title-14/chapter-I/subchapter-C/part-25`.

[15] Marc Bodson. Evaluation of optimization methods for control allocation. *Journal of Guidance, Control, and Dynamics*, 25(4):703–711, 2002. doi: 10.2514/2.4937.

[16] Johannes Stephan and Walter Fichter. Fast exact redistributed pseudoinverse method for linear actuation systems. *IEEE Transactions on Control Systems Technology*, PP:1–8, 11 2017. doi: 10.1109/TCST.2017.2765622.

[17] Simon Hafner, Stephan Myschik, Jakob Bachler, and Florian Holzapfel. Fast pseudoinverse-based control allocation using variant of cholesky decomposition. *Journal of Guidance, Control, and Dynamics*, 48(8):1901–1914, 2025. doi: 10.2514/1.G008767.

[18] Jiannan Zhang, Pranav Bhardwaj, Stefan A. Raab, Saurabh Saboo, and Florian Holzapfel. *Control Allocation Framework for a Tilt-rotor Vertical Take-off and Landing Transition Aircraft Configuration*. ISBN: 9781510868939. doi: 10.2514/6.2018-3480.

[19] Rasmus Steffensen, Agnes Steinert, Zoe Mbikayi, Stefan Raab, Jorg Angelov, and Florian Holzapfel. Filter and sensor delay synchronization in incremental flight control laws. *Aerospace Systems*, 6:1–20, 01 2023. doi: 10.1007/s42401-022-00186-2.

[20] Yagiz Kumtepe, Tijmen Pollack, and Erik-Jan Van Kampen. *Flight Control Law Design using Hybrid Incremental Nonlinear Dynamic Inversion*. ISBN: 9781624106316. doi: 10.2514/6.2022-1597.

[21] Rasmus Steffensen, Agnes Steinert, Zoe Mbikayi, Stefan Raab, Jorg Angelov, and Florian Holzapfel. Filter and sensor delay synchronization in incremental flight control laws. *Aerospace Systems*, 6:1–20, 01 2023. doi: 10.1007/s42401-022-00186-2.